

# Midwinter Suppression of Storm Tracks in an Idealized Zonally Symmetric Setting

LENKA NOVAK AND TAPIO SCHNEIDER

*California Institute of Technology, Pasadena, California*

FARID AIT-CHAALAL

*Risk Management Solutions, London, United Kingdom*

(Manuscript received 8 December 2018, in final form 3 October 2019)

## ABSTRACT

The midwinter suppression of eddy activity in the North Pacific storm track is a phenomenon that has resisted reproduction in idealized models that are initialized independently of the observed atmosphere. Attempts at explaining it have often focused on local mechanisms that depend on zonal asymmetries, such as effects of topography on the mean flow and eddies. Here an idealized aquaplanet GCM is used to demonstrate that a midwinter suppression can also occur in the activity of a statistically zonally symmetric storm track. For a midwinter suppression to occur, it is necessary that parameters, such as the thermal inertia of the upper ocean and the strength of tropical ocean energy transport, are chosen suitably to produce a pronounced seasonal cycle of the subtropical jet characteristics. If the subtropical jet is sufficiently strong and located close to the midlatitude storm track during midwinter, it dominates the upper-level flow and guides eddies equatorward, away from the low-level area of eddy generation. This inhibits the baroclinic interaction between upper and lower levels within the storm track and weakens eddy activity. However, as the subtropical jet continues to move poleward during late winter in the idealized GCM (and unlike what is observed), eddy activity picks up again, showing that the properties of the subtropical jet that give rise to the midwinter suppression are subtle. The idealized GCM simulations provide a framework within which possible mechanisms giving rise to a midwinter suppression of storm tracks can be investigated systematically.

## 1. Introduction

Most of the winter midlatitude baroclinic activity in the Northern Hemisphere is concentrated in two regions, referred to as storm tracks and located over the North Atlantic and the North Pacific. The storm tracks originate where meridional temperature gradients are sharpened by thermal contrasts between cold continents and warm western boundary currents (e.g., [Chang 2001](#)). Linear baroclinic theories going back to [Charney \(1947\)](#) and [Eady \(1949\)](#) predict that the growth rate of baroclinic eddies should be proportional to baroclinicity, which is proportional to the meridional temperature gradient divided by static stability, or to the slope of isentropes. It is then often assumed that nonlinear characteristics of storm tracks, such as the eddy kinetic energy of the equilibrated flow, should also scale with measures of baroclinicity. Over surprisingly wide ranges of climates simulated with idealized dry and

moist GCMs, this is indeed the case ([Schneider and Walker 2008](#); [O’Gorman and Schneider 2008a](#)), and it is also borne out in large-scale averages in simulations of the present climate and changed climates in comprehensive GCMs ([O’Gorman 2010](#); [Lehmann et al. 2014](#)). However, the seasonal cycle of the storm track over the North Pacific confounds this expectation.

Over the North Pacific, the climatological baroclinic eddy activity (e.g., as measured by the kinetic energy of synoptic eddies) exhibits a minimum in midwinter, when baroclinicity exhibits a maximum ([Nakamura 1992](#)). By contrast, the North Atlantic storm track is strongest in midwinter, when baroclinicity is largest, as one would ordinarily expect.

Over the North Pacific, storm-track activity increases through fall until the jet speed reaches  $\sim 45 \text{ m s}^{-1}$ . But further jet speed increases during winter are associated with weakened storm-track activity, yielding two maxima in eddy activity, one in November and one in April ([Nakamura 1992](#)). This midwinter suppression of eddy activity exhibits strong interannual variability: it is more

---

*Corresponding author:* Lenka Novak, [lenka@caltech.edu](mailto:lenka@caltech.edu)

DOI: 10.1175/JAS-D-18-0353.1

© 2019 American Meteorological Society. For information regarding reuse of this content and general copyright information, consult the [AMS Copyright Policy](#) ([www.ametsoc.org/PUBSReuseLicenses](http://www.ametsoc.org/PUBSReuseLicenses)).

pronounced during winters with stronger jets and less pronounced (or nonexistent) during winters with weaker jets (Nakamura et al. 2002). Similarly, weaker eddy activity has also been noted over the Atlantic in years with strong subtropical jets (Afargan and Kaspi 2017). Because the jet speed is related to the meridional temperature gradient through thermal wind balance, weaker eddy activity with stronger jets generally also means weaker eddy activity with stronger baroclinicity. The midwinter suppression of the Pacific storm track is a robust feature that is well captured in GCMs, even at a relatively low resolution, such as T42 and 10 vertical levels (e.g., Christoph et al. 1997; Zhang and Held 1999; Chang 2001; Robinson and Black 2005).

The midwinter suppression is also robust with respect to different diagnostics of eddy activity. It is particularly prominent in upper-tropospheric or lower-stratospheric diagnostics of synoptic eddies. For example, Nakamura (1992) characterized the suppression as a relative minimum of the geopotential height variance at 300 hPa, after applying a 6-day high-pass filter. This filter retains baroclinic activity and removes stationary waves and low-frequency variability. Another very common diagnostic for the suppression is the root-mean-square of the bandpass-filtered (e.g., 2–6.5 days) meridional velocity at 200 or 300 hPa, from which the same results can be drawn (Chang 2001; Chang et al. 2002; Lee et al. 2013). Alternatively, the suppression can be measured using Lagrangian cyclone tracking tools. For example, Penny et al. (2010) tracked individual storms using geopotential height at 300 hPa and showed that both the amplitude and frequency of storms in the Pacific storm track are reduced in winter.

In terms of its vertical extent, the midwinter suppression is also apparent in the lower troposphere, but it is less pronounced when measured by surface pressure variance or low-level meridional heat fluxes (Nakamura 1992). Schemm and Schneider (2018) used the Lagrangian approach to show that it is only the amplitude, rather than the frequency, of eddies that has a minimum during the midwinter at lower levels, contrasting with Penny et al.'s (2010) analysis of the upper levels, where both the amplitude and frequency are reduced in midwinter. This suggests that during midwinter, fewer perturbations are able to interact between the lower and upper levels, as was also suggested by Nakamura and Sampe's (2002) and Yin's (2002) observations that eddies become shallower during midwinter.

The horizontal structure of the suppression is an equatorward shift in the storm track, a strengthened subtropical jet, but weakened upper-level westerlies above the storm tracks. The latter results in a lowered tropopause and higher upper-level static stability at the storm-track

latitudes (Yin 2002; Nakamura and Sampe 2002). This equatorward shift is more apparent in the upper levels, leading to a greater meridional tilt of the eddies with height during midwinter.

Many mechanisms have been proposed to explain why linear theory is insufficient to produce the midwinter suppression and its characteristics. They can be classified into two strands, based on whether or not they require zonally asymmetric forcings of the atmosphere.

Mechanisms that require zonal asymmetries include the following:

- Penny et al. (2010) suggested that the midwinter suppression in the Pacific storm activity arises from a reduced baroclinicity over central Asia (see also Lee et al. 2013) during midwinter, owing to the high static stability over the cold continent. This was based on the fact that storms originating over the Asian continent north of 40° latitude are less frequent and weak. In contrast, storms forming over the ocean or over the continent south of 40° are more frequent and stronger during midwinter. Hence, the midwinter suppression may be attributable to reduced storm seeding upstream of the Pacific storm track.
- In support of upstream seeding argument, Park et al. (2010) additionally suggested that the Asian mountains disrupt the flow and divert wave packets equatorward, which leads to a reduction of eddy development farther downstream over the Pacific Ocean [similarly to the idealized study of baroclinic jets over topography of Son et al. (2009)]. The authors found that the midwinter suppression is substantially less pronounced in the absence of the Asian mountains. In a similar GCM study, but with an interactive ocean, Lee et al. (2013) also alluded to the importance of orography for the suppression. The authors argued that the Tibetan Plateau affects the suppression via three mechanisms: 1) inhibition of baroclinic instability because of a strengthened barotropic shear on the flank of the jet, according to the “barotropic governor” theory of James (1987); 2) decrease of baroclinicity over central Asia (as in Penny et al. 2010 and Park et al. 2010); and 3) diabatic effects pertaining to warmer SST in the western tropical Pacific.

Nevertheless, a suppression, albeit weaker, is noticeable in these studies even in the absence of orography. In addition, the upstream seeding arguments have been challenged by Chang and Lin (2011) and Chang and Guo (2012), who argued that baroclinic activity over the Pacific is decorrelated from baroclinic activity over central Asia, and by Schemm and Schneider (2018), who showed that baroclinic eddies do not decrease in frequency but only in amplitude in midwinter, suggesting

a local mechanism for the reduced eddy activity in the Pacific storm track.

- Localized diabatic heating is a primary driver of stationary waves (Chang 2009) and has also been suggested to play a role in the midwinter suppression. Chang et al. (2002) argued that immediately upstream of the Pacific storm track, moist heating over the ocean is a source of eddy available potential energy in fall and spring, while in the winter sensible cooling dominates and acts as a sink. Furthermore, Chang and Zurita-Gotor (2007) suggested that dry dynamics cannot capture the suppression entirely, with the suppression being weaker and shorter in a dry model [as was also observed in Zhang and Held (1999)].
- Nakamura (1992) suggested that locally faster winds favor a more rapid downstream propagation of the eddies in the Pacific in midwinter, leaving eddies less time to grow before leaving the zone of strong temperature gradients. However, Chang (2001) notes that this effect is likely counterbalanced by the faster cyclogenesis associated with the increased baroclinicity [agreeing with the results of Nakamura and Sampe (2002)].

Mechanisms that do not require zonal asymmetries for the existence of the midwinter suppression include the following:

- Nakamura (1992) suggested that stronger jets trap baroclinic eddies near the surface and prevent them from growing, assuming that the reduced meridional scale of baroclinic eddies (associated with a lower steering level) also translates into a reduction in the eddies' vertical scale. However, as shown in Chang's (2001) regression analysis, the wave trapping is more pronounced in the upper levels rather than the lower levels.
- Nakamura and Sampe (2002) argued that when the subtropical jet is stronger, its vorticity gradients trap upper-level disturbances entering the storm track and guide them away from the zone of low-level baroclinicity. This reduces the interaction between the upper and lower levels, inhibiting baroclinic growth. This mechanism was also suggested for the observed decrease in upper-level storm-track activity and increase in baroclinicity in the South Pacific during austral winter (Nakamura and Shimpou 2004). However, the lower-level storm track in the Southern Hemisphere forms well away from the subtropical jet in the subpolar South Pacific during austral winter.
- Yuval et al. (2018) found a correlation between the eddy kinetic energy and the latitude of the midlatitude jet in reanalysis data and an idealized dry GCM. They showed that the steady-state midwinter suppression

conditions are linked with the midlatitude jet being located farther equatorward (see also Afargan and Kaspi 2017), though the physical mechanism for this link remains unclear. The importance of latitudinal jet shifts for storm tracks is also noted by Lachmy and Harnik (2014), who showed that for regimes where the subtropical jet dominates, decoupling of upper and lower levels leads to a weakened baroclinic generation of eddy energy.

- Christoph et al. (1997) and Deng and Mak (2005) suggested that the decrease in eddy amplitude may be caused by increased barotropic deformation of the eddies due to the strong horizontal wind shear, akin to the barotropic governor theory of James (1987). Deng and Mak (2005) emphasize that such a mechanism is especially effective in a localized storm track, but it would also play a role in a zonally symmetric one. Similarly, Harnik and Chang (2004) studied the effect of the subtropical jet strength and width on baroclinic growth and concluded that a narrower and faster baroclinic jet becomes more stable. However, they argued that this alone cannot explain the midwinter suppression or the seasonal cycle of the Pacific storm track.

Thus, many mechanisms have been proposed for the existence of the midwinter suppression. While several of them may play a role in modifying the characteristics of the suppression, it is still unclear which mechanisms are the minimal ingredients for a suppression to arise. The importance of zonal asymmetries was recently challenged by Yuval et al. (2018), who reproduced the midwinter suppression by relaxing an idealized GCM to the observed temperature profile, zonally averaged over the Pacific sector. Here we build on this result and show that a midwinter suppression can arise in a statistically zonally symmetric GCM with a radiative seasonal forcing that is independent of the observed atmosphere. We also perform a sensitivity analysis that allows us to rule out several of the above mechanisms as being essential.

## 2. Observed storm tracks

We begin with a review of storm-track observations, as a backdrop for our GCM simulations. Figure 1 shows the seasonal cycles of the three main storm tracks in ERA-Interim data (Dee et al. 2011) for 1979–2016. In Fig. 1a, storm-track activity is diagnosed using the synoptic-scale variance of the meridional wind  $\overline{v'^2}$ , where the bar denotes the average of 2–6.5-day bandpass-filtered fields, and primes denote perturbations thereof [using a Butterworth filter and following the methods of Chang (2001)]. Neither the reanalysis nor the GCM analysis below are very sensitive to the precise choice of filter (e.g., using 0–8 or 0–10 days for the filtering

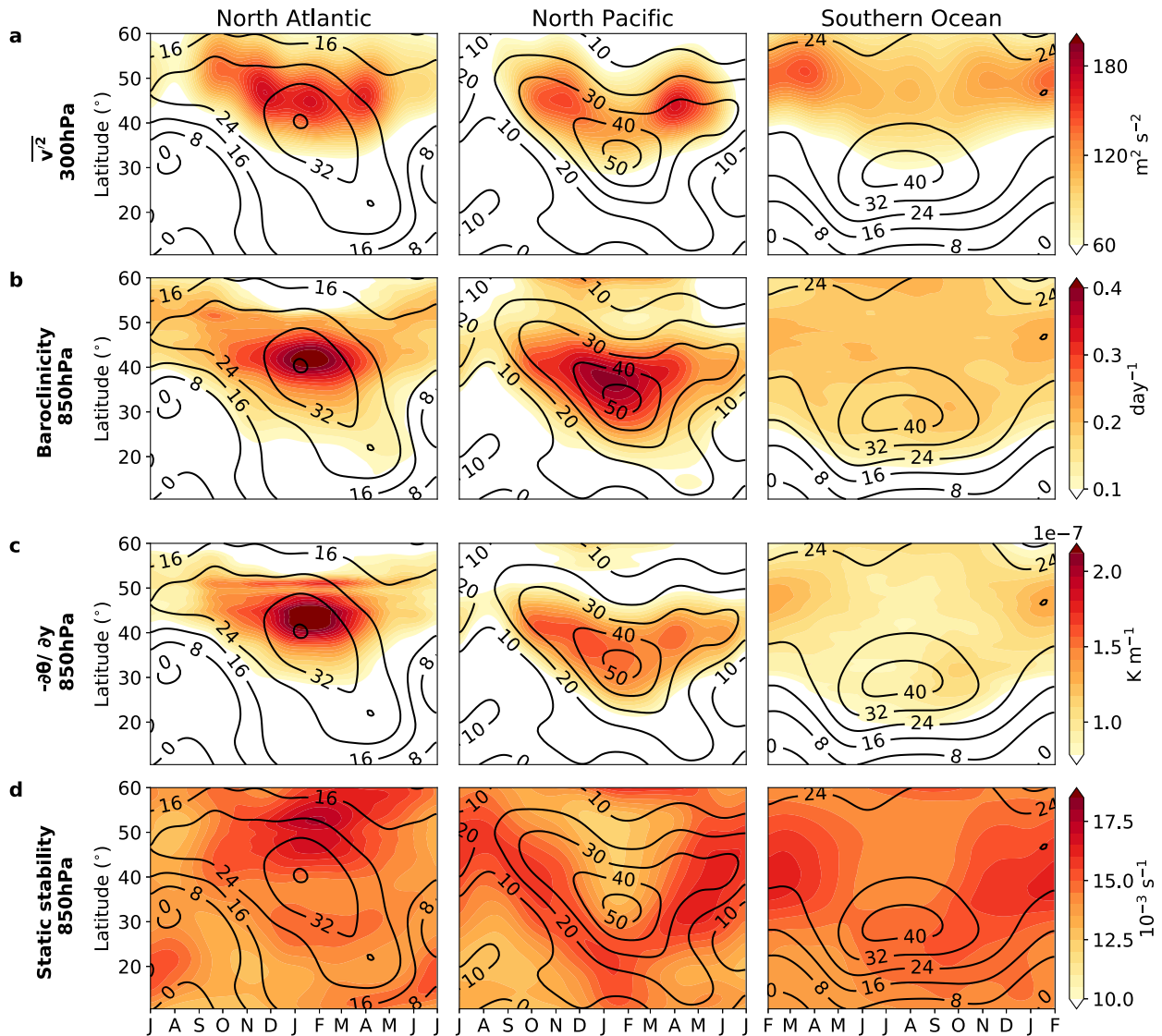


FIG. 1. Observed seasonal cycles of the (left) North Atlantic, (center) North Pacific, and (right) Southern Ocean storm tracks. (a) Meridional wind variance  $\overline{v^2}$  at 300 hPa. (b) Baroclinicity as measured by the Eady growth rate at 850 hPa. (c) Equatorward potential temperature gradient  $-\partial\theta/\partial y$  at 850 hPa. (d) Static stability  $\overline{N}$  at 850 hPa. Black contours show the zonal wind at 200 hPa ( $\text{m s}^{-1}$ ). All fields are based on ERA-Interim (see text).

window yields similar results), as long as synoptic eddy frequencies are included. For better visualization, all time series were smoothed with a 40-day Butterworth filter (similarly to Nakamura 1992). Figure 1a displays the meridional wind variance  $\overline{v^2}$  (300 hPa) and the zonal wind (200 hPa), separately for the central North Pacific (zonally averaged between 160°E and 160°W), North Atlantic (zonally averaged between 30° and 70°W), and Southern Ocean (zonally averaged along the latitude circle).

The known differences in the seasonal cycle between the North Atlantic and Pacific storm tracks are apparent: upper-level winds in midwinter over the North Pacific

are substantially stronger than over the Atlantic, but the North Atlantic exhibits stronger eddy activity. The Pacific storm track and the upper-level jet also migrate equatorward in midwinter by about 10°, whereas the storm-track latitude in the Atlantic remains almost constant through the winter. The Southern Ocean storm track is marked by a subtropical zonal wind maximum and a decrease in the maximum eddy activity in midwinter (though the eddy activity is more latitudinally dispersed); this decrease lasts around 6 months, longer than in the North Pacific. However, different sectors of the Southern Ocean exhibit different seasonal variability of eddy activity, and these sectors strongly influence

each other (Nakamura and Shimpo 2004). This makes the Southern Ocean seasonal variability more complicated. Thus, we focus on the North Pacific storm track, which is contained over the North Pacific Ocean and whose midwinter suppression has been attributed mainly to local dynamics (Schemm and Schneider 2018).

Figure 1 also shows the low-level baroclinicity (Fig. 1b; expressed as the Eady growth rate  $\propto |\partial_y \theta / N^{-1}|$ ), meridional temperature gradients (Fig. 1c), and static stability (Fig. 1d). The location of the strongest baroclinicity and temperature gradient mostly follows the location of the upper-level jet. Overall the baroclinicity increases during the suppression due to changes in both static stability and meridional temperature gradients, as reported in many previous studies.

### 3. Idealized GCM and simulation setup

We use an idealized moist primitive equation GCM based on GFDL’s Flexible Modeling System. It was used in several previous studies of large-scale dynamics (e.g., Schneider 2004; Walker and Schneider 2006; Schneider and Walker 2006; Schneider 2006; Bordoni and Schneider 2008; O’Gorman and Schneider 2008b; Schneider 2010; Kaspi and Schneider 2011, 2013; Mbengue and Schneider 2013; Levine and Schneider 2015; Chemke 2017).

The radiative parameterization consists of a two-stream gray radiation scheme (Frierson 2007; O’Gorman and Schneider 2008b). Optical thickness for longwave and shortwave radiation is time independent and prescribed as a function of pressure and latitude. In particular, the longwave optical thickness does not depend on water vapor, so that water vapor feedback is absent from the model. The top-of-atmosphere (TOA) insolation is imposed with a seasonal cycle corresponding to a 360-day circular orbit with an obliquity of 23.5°.

The boundary condition at the surface is a mixed layer slab ocean with an albedo of 0.38 and a depth of 10 m in the control run. The mixed layer exchanges radiative energy and sensible and latent heat with the atmosphere. As in Bordoni and Schneider (2008), we impose a zonally and hemispherically symmetric and time-independent ocean meridional energy flux (referred to as  $Q$  flux) to mimic oceanic heat transport in the tropics. Its structure is

$$Q = \frac{Q_s}{\cos\phi} \left( 1 - 2 \frac{\phi^2}{\delta\phi_s^2} \right) \exp\left( -\frac{\phi^2}{\delta\phi_s^2} \right), \quad (1)$$

where  $\phi$  is latitude,  $\delta\phi_s = 11.3^\circ$  characterizes width of the region of divergence around the equator, and  $Q_s$  is the heating amplitude. We set  $Q_s = 40 \text{ W m}^{-2}$  in the control run. Further details can be found in Bischoff and Schneider (2014).

To investigate whether a midwinter suppression arises in the GCM, we vary the ocean depth and the  $Q$ -flux amplitude  $Q_s$ , separately and simultaneously, forming a matrix of nine runs. The ocean depth range (6, 10, and 40 m) was chosen to represent relatively large changes to the thermal inertia of the surface, which affects the amplitude of the seasonal cycle. The ocean  $Q$ -flux range (10, 40, and 80  $\text{W m}^{-2}$ ) was chosen to induce substantial changes in low-latitude temperature gradients. We refer to the individual runs using the notation of oc10qf40, which refers to ocean depth of 10 m and  $Q$ -flux amplitude of 40  $\text{W m}^{-2}$ .

Varying these parameters allows us to assess the sensitivity of the storm-track activity suppression to the climatology of the mean circulation. Decreasing the ocean depth (i.e., thermal inertia of the surface) causes a decreased response time of the surface temperature and hence of the circulation to the radiative seasonal cycle. This leads to larger seasonal variations in meridional temperature gradients, increasing both the strength and latitude of the wintertime subtropical jet (Chen et al. 2007). This idealized setting is loosely analogous to changing the depth of the ocean mixed layer on Earth where the oceanic circulation is negligible. The equatorial  $Q$  fluxes, analogous to tropical surface heating on Earth, determine the large-scale meridional temperature gradients. As opposed to the ocean depth parameter, increasing the  $Q$  fluxes increases the latitude of the subtropical jet but decreases its strength, so the sensitivity of the suppression to either the latitude or strength of the subtropical jet can be separated.

The GCM was run at T85 resolution with 30 unevenly spaced vertical  $\sigma$  levels (where  $\sigma$  refers to the pressure divided by the surface pressure). This and lower resolutions have been found sufficient to produce realistic storm-track variability (e.g., Fraedrich et al. 2005; Mbengue and Schneider 2017; Novak et al. 2017). Eighth-order hyperdiffusion was used throughout the domain with a damping time scale of 8 h of the smallest resolved scales. Each run was 25 years long, with the first 10 years being discarded as a spinup. Because the GCM is hemispherically symmetric, the two hemispheres (offset by 180 days to take into account the seasonal cycle) were averaged together. This yielded an effective average of 30 years for each seasonal cycle. A subset of simulations was repeated for longer periods (50 years) to ensure that the runs are in a statistical steady state.

### 4. Control run

#### a. Climatology

The control simulation is run with an ocean depth of 10 m and an ocean  $Q$  flux of 40  $\text{W m}^{-2}$ . These values

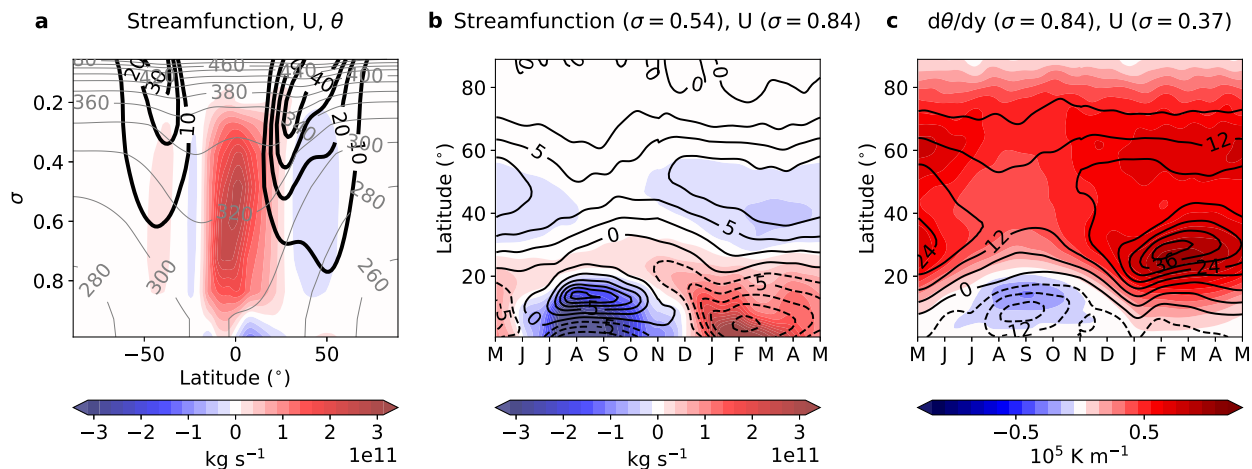


FIG. 2. Climate of control run with idealized GCM. (a) Winter (DJF) zonal-mean zonal wind (thick black contours;  $\text{m s}^{-1}$ ), meridional streamfunction (colors;  $\text{kg s}^{-1}$ ), and potential temperature (thin gray contours; K). Positive streamfunction values indicate clockwise circulation; negative values indicate counterclockwise circulation. (b) Seasonal cycle of midlevel ( $\sigma = 0.54$ ) meridional streamfunction (colors;  $\text{kg s}^{-1}$ ) and low-level ( $\sigma = 0.84$ ) zonal wind (black contours;  $\text{m s}^{-1}$ ). (c) Seasonal cycle of upper-level ( $\sigma = 0.37$ ) zonal wind (black contours;  $\text{m s}^{-1}$ ) and lower-level ( $\sigma = 0.84$ ) meridional potential temperature gradient (colors,  $10^{-3} \text{ K m}^{-1}$ ).

were chosen to reproduce a climate similar to that of the present Earth. Figure 2a shows the DJF average of zonal wind, temperature, and meridional mass flux streamfunction. In the winter hemisphere, the overturning cells are more pronounced and shifted equatorward, accompanied by a strong upper-level subtropical jet. The fields in this figure are comparable to those observed in the austral winter on Earth (e.g., Källberg et al. 2005). The signs of the zonal wind and the meridional mass flux in lower levels correlate, consistent with Ekman balance near the surface (Fig. 2b). Since the low-level zonal winds are weak in the subtropics, the upper-level winds there correlate with the local lower-level meridional temperature gradients, as expected from thermal wind balance (Fig. 2c).

There is some discrepancy in the timing of the seasonal march of the subtropical jet. The idealized GCM's atmosphere lags the radiative forcing by about 2 months. Specifically, the radiative forcing in the Northern Hemisphere peaks on 21 December in the GCM, but the midwinter (characterized by the strongest meridional overturning circulation and strongest subtropical winds) occurs in mid-February. In contrast, the Pacific midwinter takes place in mid-January. This larger lag in the GCM seasonal cycle is a result of its larger thermal inertia, which increases with the slab ocean depth and is further enhanced by the absence of continents (Bordoni and Schneider 2008; Merlis et al. 2013). This bears implications for the spring circulation, including the onset and termination of the midwinter suppression, as we will discuss in section 6.

The relative positions of the subtropical and stratospheric jets in the GCM also differ from the North Pacific.

In the North Pacific, the stratospheric jet is more poleward and less connected to the tropospheric subtropical jet. However, since the eddy activity in the upper troposphere predominantly consists of waves propagating upward from the lower troposphere (as evidenced by the positive meridional eddy heat fluxes shown below; Edmon et al. 1980), the influence of the stratosphere on the tropospheric eddy growth is generally weak. Thus, this GCM is still appropriate to investigate the general characteristics of winter storm-track variability, such as the midwinter suppression.

Note that in cases with two zonal wind maxima in the same hemisphere, we refer to the equatorward maximum (near  $30^\circ$  latitude) as the “subtropical jet” and the more poleward maximum (near  $50^\circ$  latitude) as the “midlatitude jet,” without identifying what mechanism drives them. We refrain from the “eddy-driven jet” terminology, since both the subtropical and midlatitude jets are shaped by eddies (e.g., Schneider 2006; Levine and Schneider 2015; Ait-Chaalal and Schneider 2015).

### b. Midwinter suppression

Figure 3 shows the storm-track activity in the control run using different diagnostics, namely,  $\overline{v'^2}$ ,  $\overline{\theta'^2}$ , and  $\overline{u'^2}$  in the upper levels ( $\sigma = 0.37$ ), and  $\overline{v'\theta'}$  in a lower level ( $\sigma = 0.84$ ). As above, these were obtained using a 2–6.5-day bandpass filter and a 40-day low-pass smoothing. These and similar diagnostics have been used in previous studies. The midlatitude midwinter suppression is apparent in all cases. An investigation of the vertical profiles confirmed that the suppression is not a result of the eddy maxima moving vertically (Fig. 9). The upper-level

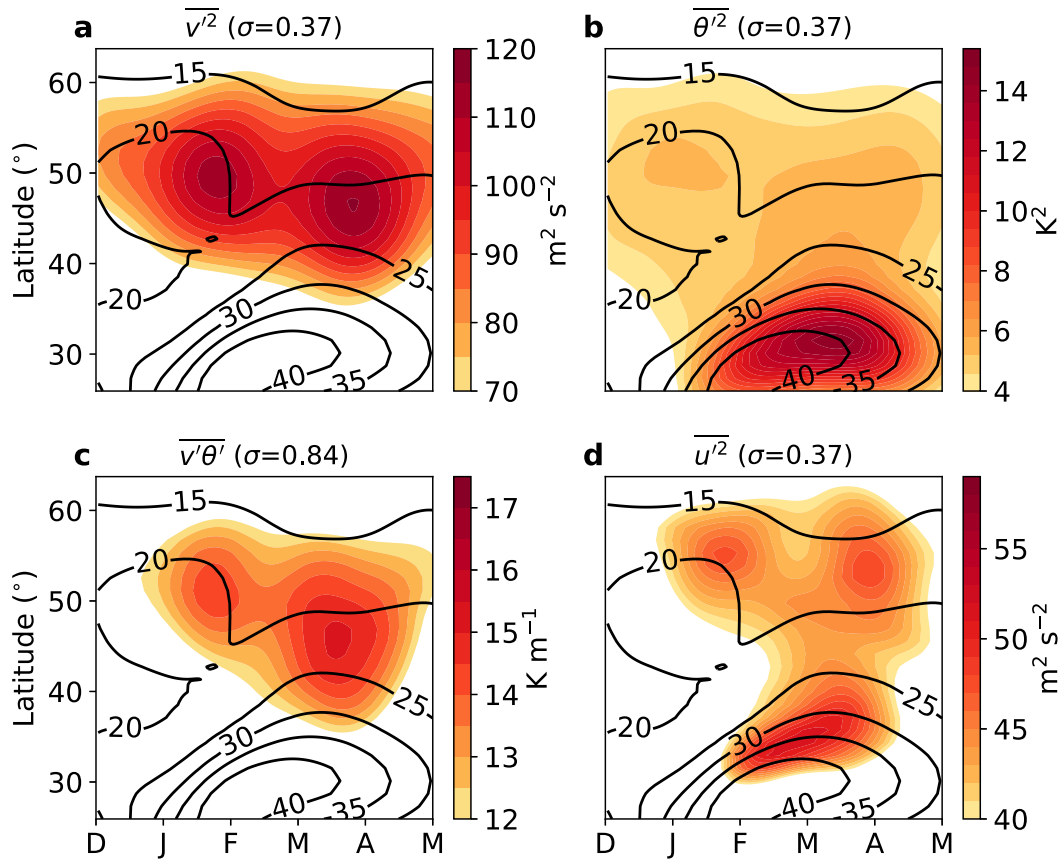


FIG. 3. Midwinter suppression in storm-track activity from the control run (oc10qf40). Colors indicate (a) upper-level meridional velocity variance  $\overline{v'^2}$  at  $\sigma = 0.37$ , (b) upper-level potential temperature variance  $\overline{\theta'^2}$  at  $\sigma = 0.37$ , (c) lower-level meridional heat flux  $\overline{v'\theta'}$  at  $\sigma = 0.84$ , and (d) upper-level zonal velocity variance  $\overline{u'^2}$  at  $\sigma = 0.37$ . The upper-level ( $\sigma = 0.37$ ) zonal wind is shown with black contours. Eddies are determined with a 2–6.5-day bandpass filter.

$\overline{\theta'^2}$  and  $\overline{u'^2}$  have additional midwinter maxima near the poleward flank of the subtropical jet, which are not associated with a maximum in  $\overline{v'^2}$ . These maxima are most likely associated with pulsations of the poleward flank of subtropical jet, rather than synoptic eddy activity. The storm-track activity amplitudes and latitudinal shifts are comparable to their observational counterparts in the Southern Ocean, but the timing of the GCM suppression is later in the winter, owing to the lagged atmospheric response to the higher surface thermal inertia, discussed above. The duration of the GCM suppression is shorter than in both the Southern Ocean and the North Pacific. In the GCM it lasts for approximately two months. Since  $\overline{v'^2}$  shows the clearest suppression, we focus on this diagnostic in the analysis of the midwinter suppression characteristics below.

Figure 3 additionally includes the upper-level zonal-mean zonal wind, showing that the midlatitude jet (at around 50° latitude) collapses with the onset of the suppression, after which the subtropical jet (at around 30° latitude) begins to dominate.

The suppression is very similar in the long (50 years) run, as shown in the appendix, indicating that the 30-yr averages represent the steady state. Any reasonable width of the low-pass filter used to smooth the final time series yields the midwinter suppression. In the appendix we show that that the suppression is apparent even if the time series is unfiltered, though the additional noise makes the suppression less pronounced.

c. Vertical structure and eddy frequency

The vertical dependency of the midwinter suppression is shown in Figs. 4a–c. The suppression is not apparent in low levels and is weak above the tropopause. However, if the filtering window is extended to include eddies with time scales of 2–15 days (bottom row), the suppression is also seen in low levels. Additionally, the same plots for eddies with time scales of 6.5–15 days (Figs. 4d–f) show that lower-frequency eddies are most active during the fall maximum, whereas higher-frequency eddies are most active during the spring maximum. This suggests that the eddies contributing to the two maxima are, on average, of

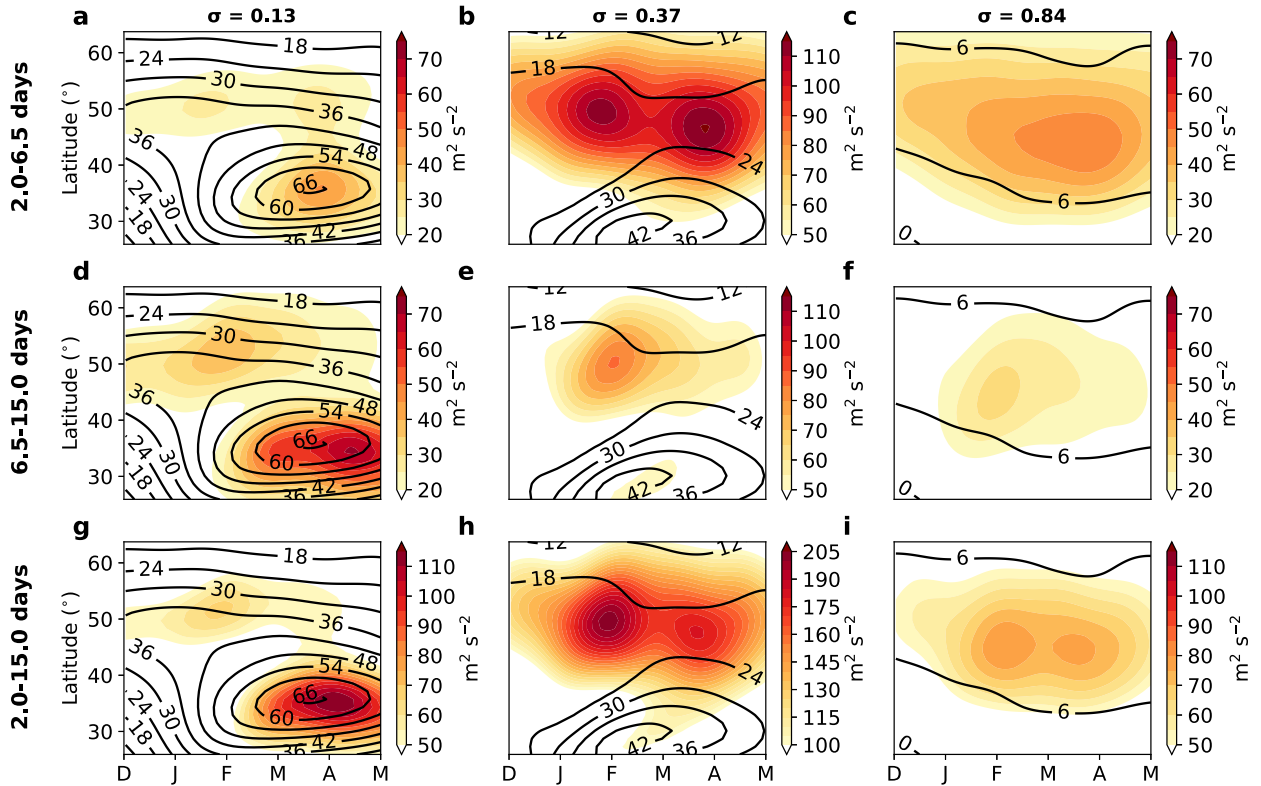


FIG. 4. Vertical dependency of the seasonal variability of meridional velocity variance  $\overline{v'^2}$  from the control run (oc10qf40) in the (left) lower stratosphere ( $\sigma = 0.13$ ), (center) upper troposphere ( $\sigma = 0.37$ ), and (right) lower troposphere ( $\sigma = 0.84$ ). Eddies are determined with bandpass filters with time scales of (a)–(c) 2–6.5, (d)–(f) 6.5–15, and (g)–(i) 2–15 days. Black contours are the zonal-mean zonal wind at that level.

different scales, both temporal and spatial since the two are largely proportional to each other for baroclinic eddies (Solomon 1997). This is also supported by Lachmy and Harnik (2016), who used a two-layer quasigeostrophic model to find that a merge of the subtropical and midlatitude jets produces higher wavenumbers compared to when the jets are not merged. These studies and the results above imply that the GCM suppression is characterized by a transition from a regime dominated by the midlatitude jet to a regime dominated by a merged jet in the subtropics (to which we refer as the subtropical jet here).

At the stratospheric level (Figs. 4a,d,g), the storm track exhibits an equatorward shift due to a shallow secondary maximum in eddy activity at the latitude of the subtropical jet. This eddy activity is much stronger for the lower-frequency waves, which penetrate more easily across the tropopause (e.g., Charney and Drazin 1961; James 1994). The structure of the midwinter suppression is not vertically constant, reflecting the changes in the structure of the zonal wind shown above. Nevertheless, the suppression is still apparent if the diagnostics above are vertically integrated (see the appendix).

#### d. Eddy energy source

The asymmetry between the shoulder seasons around the GCM suppression shown in the previous section indicates that the subtropical jet plays a crucial role in triggering the suppression. The analysis of eddy time scales indicates a change in the source of eddy energy. To explore this explicitly, we analyze the tendency equation of eddy energy  $E$ , defined as the sum of eddy kinetic energy,  $(1/2)\langle \overline{u'^2} + \overline{v'^2} \rangle$ , and eddy available potential energy,  $(1/2)\langle c_p \gamma \overline{\theta'^2} \rangle$ . The evolution equation of the global eddy energy is (e.g., following Lorenz 1955):

$$\frac{\partial E}{\partial t} = \left\langle c_p \gamma \overline{v' T'} \frac{\partial \overline{T'}}{\partial y} \right\rangle - \left\langle \overline{u' v'} \frac{\partial \overline{u}}{\partial y} \right\rangle + \mathcal{R}, \quad (2)$$

where  $u$  and  $v$  are the zonal and meridional wind components,  $T$  is temperature, and  $\mathcal{R}$  refers to the residual, primarily consisting of diabatic and frictional sources and sinks. In Eq. (2), the stratification parameter is defined as

$$\gamma = \frac{\theta}{T} \frac{R}{c_p p} \left( \frac{\partial \Theta}{\partial p} \right)^{-1},$$

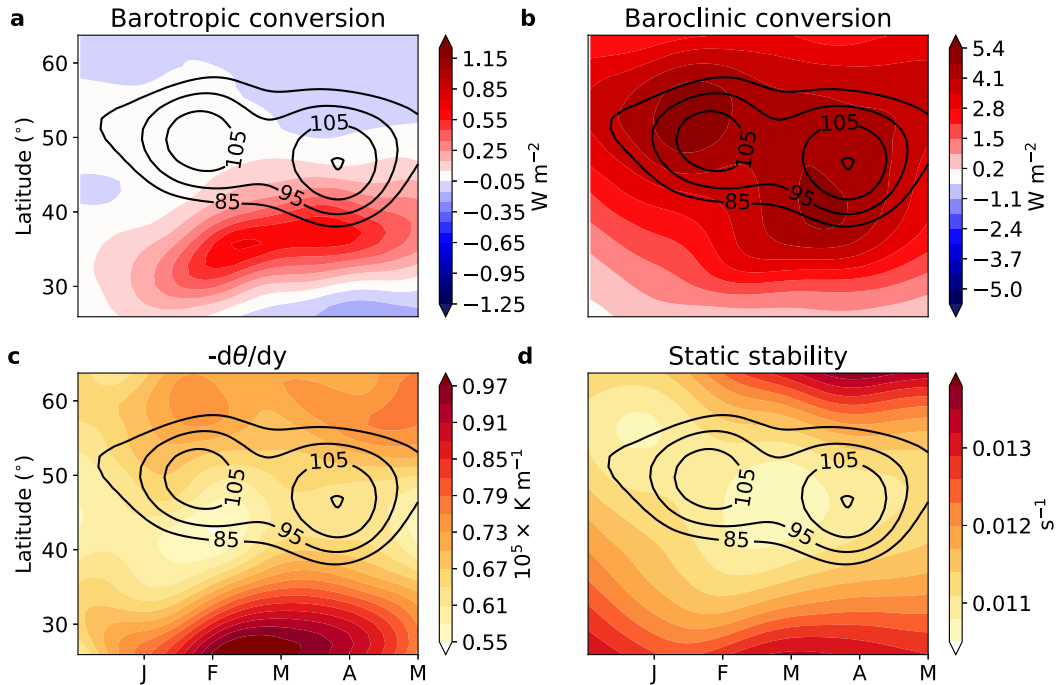


FIG. 5. Seasonality of the conversion terms in the Lorenz energy cycle from the control run (oc10qf40). (a) Vertically integrated barotropic conversion from mean to eddy kinetic energy. (b) Vertically integrated baroclinic conversion from mean to eddy potential energy. (c) Meridional potential temperature gradient (850 hPa). (d) Static stability (850 hPa). The black contours show the meridional velocity variance  $v^2$  at  $\sigma = 0.37$  for 2–6.5-day eddies, as in Fig. 4b.

where  $p$  is pressure,  $R$  is the specific gas constant for dry air,  $\theta$  is potential temperature,  $\Theta$  is potential temperature area averaged on pressure surfaces over a hemisphere, and  $c_p$  is the specific heat at constant pressure. The overbars denote time averaging (in this case bandpass-filtered time series) and primes denote the perturbations thereof. The angle brackets denote mass integrations over the hemispheric domain. The first term in Eq. (2) is the (baroclinic) energy conversion from mean available potential energy and the second term is the (barotropic) conversion from the mean kinetic energy. The mean energy refers to the energy of the large-scale, slowly varying flow.

Computing  $\mathcal{R}$  as a residual of the rest of the terms in Eq. (2) reveals that only the conversion terms act as substantial sources of energy in the climatological seasonal cycle, whereas  $\mathcal{R}$  is overall negative (i.e., dissipating eddies). In this investigation of sources and sinks of eddy energy, we also omit discussing the transport terms, which merely redistribute the eddy energy, vanish upon global averaging, and are relatively small averaged over storm-track sectors. Figure 5 therefore only shows the seasonality of the latitudinal distribution of the conversion terms. It is evident that the barotropic conversion process alone cannot be responsible for the suppression.

Though a significant barotropic kinetic energy conversion from mean flow to eddies occurs during the spring maximum (when the horizontal wind shear is opposite compared to the rest of the year due to the encroaching subtropical jet), there is no reduction of this term at the time of the midwinter suppression (Fig. 5a).

On the other hand, the baroclinic conversion does mirror the changes in the storm track, as was found by Chang (2001) and Yin (2002). These studies attributed the existence of the suppression to a reduction in the baroclinic conversion. However, this conversion term is proportional to the geometric mean of the kinetic and available potential energy of the eddies themselves (Schneider and Walker 2008), and so causality is difficult to identify from this term alone. Nevertheless, this term is insightful for showing that the source of eddy energy is concentrated on the poleward side of the storm track before the suppression and on the equatorward side after the suppression. This conversion responds mainly due to the meridional temperature gradient in Eq. (2), which drives the low-level linear growth rate and appears to dominate over the changes in static stability (Figs. 5c,d).

The baroclinic eddy growth during the fall maximum is associated with high baroclinic conversion poleward

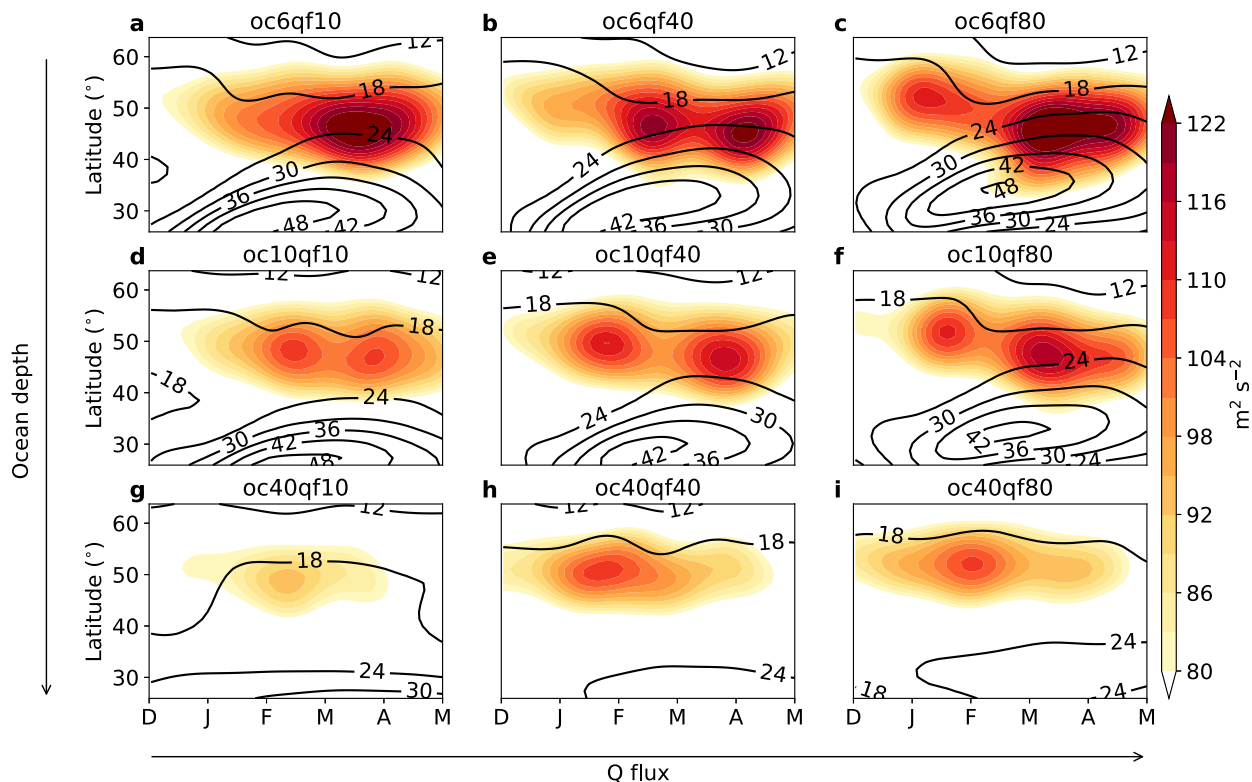


FIG. 6. Sensitivity in the GCM runs of the seasonal variability of  $\overline{v^2}$  (colors; at  $\sigma = 0.37$ ) and zonal wind (black contours; at  $\sigma = 0.37$ ) to changing  $Q$  fluxes and ocean depth. Eddies were computed using filter time scales of 2–6.5 days. (e) The control run.

of the storm track, and a weak barotropic eddy decay through barotropic energy conversion from eddies to the mean flow, consistent with the classical baroclinic eddy life cycle studies (Simmons and Hoskins 1978; Thorncroft et al. 1993). Following the suppression, the subtropical jet dominates eddy growth in two ways. The jet is strong and deep enough, so that the low-level meridional temperature gradient and hence baroclinic eddy growth are enhanced. The subtropical jet also introduces a negative horizontal shear to the region of poleward eddy westerly momentum fluxes during and following the suppression, which reverses the sign of the barotropic conversion and thus yields barotropic eddy growth (this is also the case during the Pacific suppression).

### 5. Sensitivity to mean flow characteristics

We study further characteristics of the midwinter suppression and the role of the subtropical jet in the GCM by varying the ocean depth and tropical ocean heating ( $Q$  flux). Figure 6 shows that the suppression (i.e., the decrease in eddy energy in February) can appear and disappear by varying one or both of these parameters. The figure also shows that the spring maximum is most

prominent for runs where the subtropical jet is strongest and most poleward. As a result of this, the midwinter suppression often becomes more prominent. This can be achieved solely by decreasing the ocean depth, which decreases the thermal inertia of the surface and enhances the seasonal cycle. However, the subtropical jet strength and latitude are not proportional when the  $Q$  flux is varied, and a too weak or too equatorward subtropical jet can be associated with the suppression becoming less prominent. For example, the jet of run oc6qf10 is stronger but more equatorward than the jets of runs oc6qf40 and oc6qf80. This results in a less pronounced midwinter suppression in run oc6qf10. In general, the suppression tends to occur for a sufficiently high  $Q$  flux and a sufficiently shallow ocean.

The sensitivity of the properties of the midwinter suppression to the ocean depth and heating in the GCM can be summarized as follows:

- *Duration.* The midwinter suppression lasts for up to 60 days. Since the suppression in the GCM is terminated by the subtropical jet encroaching on the mid-latitude storm track in spring, the duration of the suppression is highly dependent on the subtropical jet strength and its seasonal shifts with latitude. If the jet

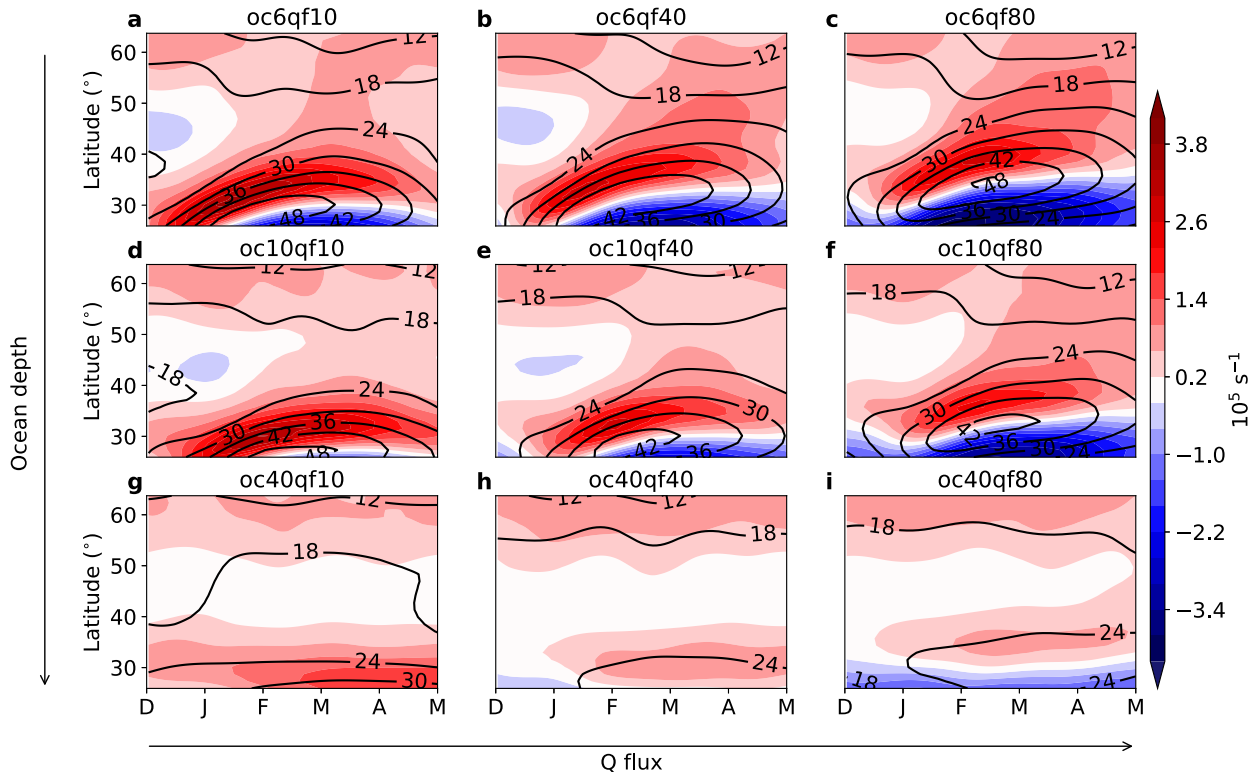


FIG. 7. As in Fig. 6, but for the equatorward zonal wind shear (colors;  $\text{m s}^{-1}$  over 100 km at  $\sigma = 0.37$ ) and zonal-mean zonal wind (black contours; as in Fig. 6).

moves poleward too early in winter, the fall and spring maxima merge and the suppression becomes less pronounced.

- *Different eddy scales.* The midwinter suppression is characterized with a transition to more active higher-frequency eddies, as in the control run.
- *Shift in the storm-track latitude.* Storm-track activity starts shifting equatorward during the suppression and continues to shift into the spring. For higher  $Q$  fluxes the transition is more abrupt (Fig. 6).
- *Subtropical jet becomes dominant.* All suppressions in these sensitivity runs coincide with a strengthening of the subtropical jet, a weakening of the midlatitude jet, and a reversal in the horizontal zonal wind shear in the storm-track region (Fig. 7). The spring maximum in storm-track activity is stronger relative to the fall maximum in the runs with a particularly strong and poleward subtropical jet (e.g., Fig. 6), which additionally supports that the subtropical jet modulates the storm track during (and following) the storm-track activity suppression.
- *Shift in the source of eddy energy.* As in the control run, only the baroclinic conversion contributes to the fall maximum, and both baroclinic and barotropic conversions contribute to the spring maximum. Again, this

is clearer in runs with large  $Q$  fluxes and shallow oceans (e.g., as can be deduced from Figs. 6 and 7).

### 6. Discussion

The results above reveal that there is an asymmetry between the shoulder seasons of the midwinter suppression in the GCM. While this asymmetry is not apparent in the midwinter suppression observed over the North Pacific, the onsets of the GCM suppressions share similar characteristics with the observed onset. Conversely, the terminations of the observed and GCM suppressions are different and caused by different processes. Below we therefore describe separately the onsets and terminations of midwinter suppressions, as well as discussing the wider implications of the above results for the existence of the midwinter suppression.

#### a. Onset

In the late fall, the GCM storm-track transitions from being dominated by the midlatitude jet to being dominated by the subtropical jet. The transition between the dominance of the two jets is not smooth. When the subtropical jet extends sufficiently poleward, the midlatitude jet collapses, and the subtropical jet becomes

dominant rather abruptly [in accordance with the experiments of Lachmy and Harnik (2016)]. The jet transition is associated with the storm track moving equatorward (which is especially apparent in the stratosphere), and with an increase in higher-frequency eddy activity relative to lower frequency. The midlatitude upper-level meridional wind shears change sign (Fig. 7), and the midlatitude tropopause is lowered (not shown).

Thus, the suppression onset seems to be intimately linked with the latitude of the dominant jet in the GCM and a transition from the midlatitude jet to a merged jet in the subtropics. Lachmy and Harnik's (2014) idealized quasigeostrophic model suggests that such a jet transition is associated with potential vorticity gradients reversing in low levels (due to a larger beta at low latitudes), which inhibits baroclinic eddy generation there. So while the eddies are trapped by the subtropical jet at low latitudes, they are unable to grow despite the strong underlying low-level baroclinicity (i.e., large meridional temperature gradients and low static stability).

This eddy-trapping mechanism has also been suggested for the onset of the North Pacific suppression (Nakamura and Sampe 2002), where a similar transition to weaker and more equatorward eddies seems to be associated with a merging of two upper-level jets and a lowered tropopause (e.g., Chang 2001; Yin 2002). However, the North Pacific subtropical jet is much weaker compared to the GCM before the suppression occurs.

Additionally, although similar processes appear to govern the onsets of the GCM and North Pacific suppressions, due to the aforementioned effect of a larger thermal inertia of the GCM surface, the GCM suppression often occurs later (i.e., late winter/early spring) than the average North Pacific suppression (though in some years, e.g., 1998, the North Pacific suppression also occurred in late winter). Nevertheless, asserting whether the onsets do have the same origin would require further investigation with more complex models that have seasonal cycles more similar to their observed counterparts.

### b. Termination

The termination (i.e., the spring maximum) in the Pacific storm track seems to be caused by a retreat of the subtropical jet and a reversal to the fall regime, which is dominated by the midlatitude jet. This can be inferred from the similarity between the circulations of the fall and spring seasons (e.g., Chang 2001; Yin 2002; Yuval et al. 2018).

In the GCM, on the other hand, the seasonal movement of the subtropical jet latitude is more pronounced and delayed due to the larger thermal inertia of the GCM surface (as discussed above), so the jet remains strong and moves poleward well into the spring. This

reinvigorates eddy activity, just poleward of this jet. It makes the GCM spring substantially different from the GCM fall and the North Pacific fall and spring, when the midlatitude jet is collocated with the storm track. In the GCM, once the spring subtropical jet reaches sufficiently poleward latitudes (where it can generate baroclinic growth more easily) the suppression is terminated, even if the speed of the subtropical jet continues to increase. The timing of the termination appears to be a function of the climatological subtropical jet; in general, the stronger and more poleward the jet, the sooner the suppression will be terminated.

### c. Existence

Although the GCM termination does not replicate the observed terminations, it is still useful for exploring some of the current theories for the existence of the suppression. Indeed, some of the main theories for the midwinter suppression are related to the subtropical jet strength and its horizontal shear. One theory is that the strong subtropical jet advects eddies away from the region of growth too quickly so that the residence time of growing eddies in the baroclinic zone is reduced (Chang 2001). This effect may also apply in zonally symmetric storm tracks, which have local (but transient) maxima of baroclinicity. However, it is evident that in some runs (e.g., oc6qg80 in Fig. 6c) the suppression occurs before the strongest zonal winds are reached. It was also argued by Nakamura and Sampe (2002) that this effect is too weak to counteract the changes in the baroclinic growth rate in the North Pacific.

Another theory, the barotropic governor (James 1987; Deng and Mak 2005), requires that the midwinter suppression occurs when the horizontal wind shear is largest. However, the timing of the suppression is not always exactly collocated with the timing of the strongest horizontal wind shear in the GCM (e.g., Figs. 6c and 7c). This is also apparent in analysis of individual years (not shown).

The above results suggest that, although the presence of the subtropical jet is essential for the GCM midwinter suppression, the advection and barotropic governor theories are insufficient to explain the suppression in the GCM. A more likely candidate is the timing of the transition from one dominant jet to another, and the associated latitudinal shifts in the circulation.

To test whether this could be the case for the North Pacific suppression, we have analyzed the relationship between eddy energy and zonal wind at each latitude for all days of the reanalysis time series longitudinally averaged over the North Pacific sector. The colored shading of Fig. 8a shows that for a given latitude, there is always a positive relationship between the zonal wind and eddy energy, even beyond the  $45 \text{ m s}^{-1}$  threshold

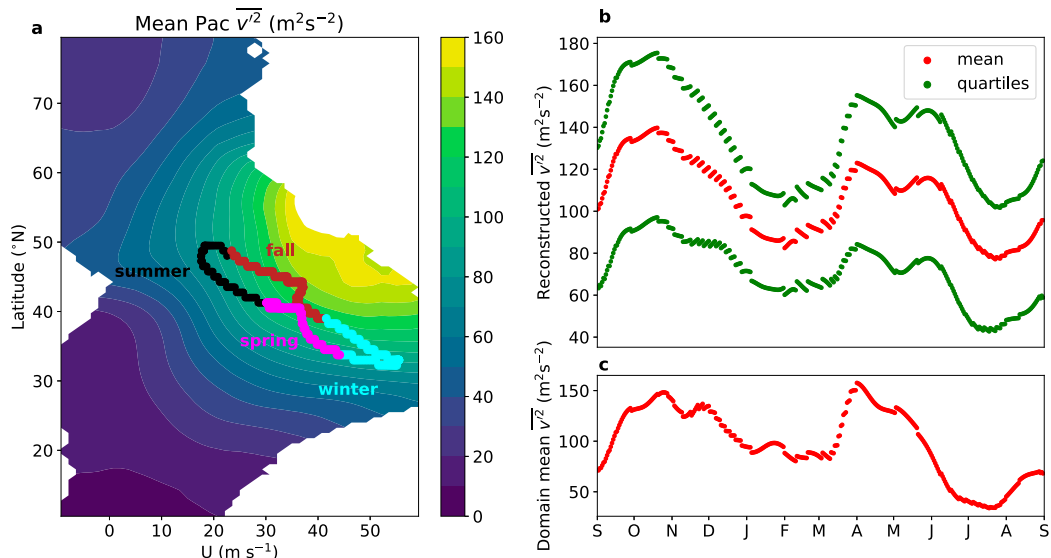


FIG. 8. Dependence of the observed (ERA-Interim) Pacific storm track on the strength and latitude of the dominant jet at 300 hPa: (a)  $\overline{v^2}$  vs zonal wind  $U$  at a given latitude. The daily time series of  $\overline{v^2}$  and  $U$  were first zonally averaged over the North Pacific sector and 40-day low-pass filtered. The magnitude of  $U$  at all times and latitudes was divided into 70 bins. Then, all  $\overline{v^2}$  data points belonging to the same latitude and  $U$  bin were averaged and interpolated in the  $U$ –latitude plane (colors), omitting averages with fewer than five data points. The scatter points show the seasonal variability of the latitude and amplitude of the dominant climatological jet (diagnosed as the daily climatology of  $U$  averaged over the Pacific sector). The colors indicate the seasons. (b) Seasonal variability of  $\overline{v^2}$  reconstructed from the latitude and strength of the dominant jet shown in (a). The mean  $\overline{v^2}$  (red) and corresponds to the colors under the scatter points in (a). The equivalent upper and lower quartiles were equivalently calculated, interpolated and reconstructed (green). (c) Observed daily climatology  $\overline{v^2}$  (spatially averaged:  $10^{\circ}$ – $70^{\circ}\text{N}$ ,  $160^{\circ}\text{E}$ – $160^{\circ}\text{W}$ ).

above which the storm-track activity was previously deemed to decrease (e.g., Nakamura 1992). The scatter points are the latitudinal locations and speeds of the dominant climatological jet (measured by the maximum zonal wind averaged over the North Pacific sector) throughout the seasonal cycle. Using a  $70 \times 70$  grid to discretize the latitude–speed plane and extracting the interpolated values of  $\overline{v^2}$  for each scatter point yields a seasonal reconstruction of the storm-track activity (Fig. 8b). The result is remarkably similar in structure to the observed hemispherically averaged storm-track activity in winter (Fig. 8c). The amplitudes in Figs. 8b and 8c are different, since the reconstruction and the observations are based on different averaging methods. These results suggest that a decrease in eddy energy during the North Pacific midwinter suppression requires a latitudinal shift in the dominant jet, rather than jet speed increasing beyond a particular threshold, agreeing with the suggestions of Nakamura and Sampe (2002) and Yuval et al. (2018).

### 7. Conclusions

This study has investigated the midwinter suppression in a moist idealized GCM with zonally symmetric

forcings. It has shown for the first time that zonal asymmetries are not necessary to produce the midwinter suppression in an atmosphere undergoing a seasonal cycle. Yuval et al. (2018) have already shown that it is possible to reproduce the Pacific midwinter suppression by forcing a zonally symmetric GCM toward the climatological temperature profile averaged over the Pacific sector. Our study builds on their results, in that it shows how a midwinter suppression can be obtained independent of the specific Pacific configuration and how, by varying GCM parameters, one can go continuously from a situation with a midwinter suppression to one without.

The amplitude and duration of the suppression can be modified by varying the tropical meridional ocean heat transport or the thermal inertia of the surface. These results rule out the mechanisms that require zonal asymmetries as necessary conditions for the suppression in the GCM, as in Yuval et al. (2018). These mechanisms include reduction of downstream development, upstream seeding from the continents, zonal advection out of a zonally confined baroclinic zone and diabatic effects due to the land–sea contrast. While such mechanisms may play a role in the climate system, they

are not essential for the suppression. Other mechanisms, which we found are also not essential for the suppression in the GCM, include the following:

- 1) *Excessive zonal advection by the strong winds away from longitudes of high baroclinicity.* In several runs, the maximum strength of the zonal wind within the storm track does not always occur at the same time as the suppression. This agrees with the analysis of the North Pacific storm track (Chang 2001; Nakamura and Sampe 2002) that this mechanism alone is insufficient to cause the suppression.
- 2) *Barotropic governor.* The horizontal wind shear strength is not symmetric around the suppression, and in some runs it lags behind the suppression by several days. This mechanism is therefore also insufficient on its own.

In contrast, what appears to be essential for the suppression in the GCM is the transition to the dominance of the subtropical jet. The encroachment of the subtropical jet into midlatitudes occurs in all storm tracks (both modeled and observed) that exhibit the midwinter suppression. Once the storm track moves equatorward, eddies change their characteristics in accordance with the newly dominating jet. Essentially, during the suppression, the storm track impinges on the poleward flank of the subtropical jet as the eddies become trapped within it (as found by Nakamura and Sampe 2002). Our GCM sensitivity runs (Fig. 6) revealed that the suppression duration coincides with the timing of the interaction between the subtropical jet and the storm track. This interaction depends on the latitudes of the climatological jets and storm tracks, as well as the strength of the subtropical jet. We have not been able to find cases where the subtropical jet interference with the storm track did not play a role in the midwinter suppression. While we do not establish the precise mechanisms responsible for the midwinter suppression here, our results demonstrate that whenever the suppression occurs (either in the GCM or in the Pacific storm tracks), the subtropical jet is strong and/or located far poleward.

The shift from a midlatitude to a subtropical jet regime has also been favored by several recent studies (Nakamura and Sampe 2002; Yuval et al. 2018) as the essential factor for the North Pacific suppression. Additionally, idealized studies (James 1987; Lachmy and Harnik 2014) show that the equatorward subtropical jet is affected by a larger beta parameter, which reduces the growth rate and size of baroclinic eddies within that jet compared to more poleward jets. We have shown explicitly that equatorward shifts in the dominant jet coincide with the suppression in eddy energy in both the

North Pacific and the GCM. The GCM runs further showed that a strong subtropical jet is capable of producing strong eddy energy as long as it is sufficiently poleward and thus meridionally aligned with the low-level baroclinic zone. This, along with the dominance of the baroclinic energy conversion term, highlights that the suppression is a result of baroclinic growth responding to latitudinal shifts of the dominant jet.

A limitation is the simplicity of the idealized GCM. With frictional and diabatic processes being highly idealized, the GCM exhibits an excessively delayed response of the circulation to the radiatively forced seasonal cycle. Such a delay manifests itself in the spring season, which is dominated by the subtropical jet in the GCM (while the observed North Pacific storm track in spring is under the dominant influence of midlatitude circulation). Although the termination of the suppression is different in the GCM due to its delayed seasonal response, the onsets in both the GCM and the North Pacific have similar characteristics, indicating a similar origin. Also, the climatological storm track in the GCM is positioned at higher latitudes, compared to the Pacific, but thanks to the enhanced seasonal latitudinal shifting of the subtropical jet in the GCM, the suppression can still occur. In other words, over the North Pacific, the storm track shifts more toward the subtropical jet, whereas in the GCM the subtropical jet shifts more toward the storm track. Both of these scenarios apparently lead to a midwinter suppression. Nevertheless, although the GCM suppressions can be obtained without zonally asymmetric forcings, firmly establishing the extent to which zonal asymmetries affect the North Pacific suppression would require more targeted sensitivity experiments in more realistic models.

Another shortcoming is that the definition of baroclinicity (as in many previous studies) is independent of the latitudinal position of the eddies. The results above suggest that the latitudinal position of the dominant jets (and thus storm tracks) is crucial for determining whether the suppression occurs. It is therefore possible that the conundrum of the North Pacific storm-track activity suppression occurring at times of highest baroclinicity may be resolved simply by redefining baroclinicity to include latitudinal dependence.

With most climate models predicting that the subtropical jet will shift poleward in the future (Kang and Lu 2012; Vallis et al. 2015), it is very likely that the midwinter storminess and precipitation over the North Pacific will also be modulated. In addition, given the mean bias of current climate models to produce too equatorward and untilted jets, it is possible that there are large biases in the onset of the midwinter suppression and its duration. This would have implications

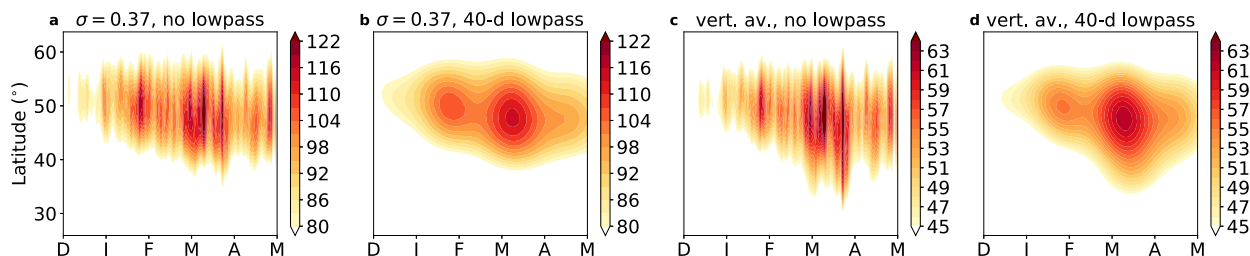


FIG. A1. Seasonal variability of synoptic (2–6.5-day)  $\overline{v^2}$  from the control run integrated over 50 years. (a) Unfiltered fields from upper levels ( $\sigma = 0.37$ ). (b) The 40-day low-pass-filtered fields from upper levels. (c) Unfiltered vertically averaged fields. (d) The 40-day low-pass-filtered and vertically averaged fields.

for the future predictions of extreme windstorms and precipitation events over the west coast of North America, and likely also in the Southern Hemisphere and Europe.

**Acknowledgments.** This work was supported by NSF (AGS-1760402). We thank Prof. Simona Bordoni, Dr. Tobias Bischoff, and Dr. Yair Cohen for useful discussions when producing the manuscript.

## APPENDIX

### Long Simulation with Control-Run Parameters

We repeated the control run for a longer period (50 years) to show that the suppression is stationary and persistent on longer time scales. Figure A1 shows the suppression for the unfiltered 2–6.5-day upper-level ( $\sigma = 0.37$ ) eddies, 40-day low-pass-filtered 2–6.5-day upper-level ( $\sigma = 0.37$ ) eddies, and 40-day low-pass-filtered 2–6.5-day vertically averaged eddies. The vertical structure of the suppression means that the vertically integrated eddy activity yields a less pronounced suppression. The absence of the low-pass filter allows for additional noise that also slightly obscures the suppression. Nevertheless, the suppression is apparent in all cases.

## REFERENCES

- Afargan, H., and Y. Kaspi, 2017: A midwinter minimum in North Atlantic storm track intensity in years of a strong jet. *Geophys. Res. Lett.*, **44**, 12 511–12 518, <https://doi.org/10.1002/2017GL075136>.
- Ait-Chaalal, F., and T. Schneider, 2015: Why eddy momentum fluxes are concentrated in the upper troposphere. *J. Atmos. Sci.*, **72**, 1585–1604, <https://doi.org/10.1175/JAS-D-14-0243.1>.
- Bischoff, T., and T. Schneider, 2014: Energetic constraints on the position of the intertropical convergence zone. *J. Climate*, **27**, 4937–4951, <https://doi.org/10.1175/JCLI-D-13-00650.1>.
- Bordoni, S., and T. Schneider, 2008: Monsoons as eddy-mediated regime transitions of the tropical overturning circulation. *Nat. Geosci.*, **1**, 515–519, <https://doi.org/10.1038/ngeo248>.
- Chang, E. K., 2001: GCM and observational diagnoses of the seasonal and interannual variations of the Pacific storm track during the cool season. *J. Atmos. Sci.*, **58**, 1784–1800, [https://doi.org/10.1175/1520-0469\(2001\)058<1784:GAODOT>2.0.CO;2](https://doi.org/10.1175/1520-0469(2001)058<1784:GAODOT>2.0.CO;2).
- , 2009: Diabatic and orographic forcing of northern winter stationary waves and storm tracks. *J. Climate*, **22**, 670–688, <https://doi.org/10.1175/2008JCLI2403.1>.
- , and P. Zurita-Gotor, 2007: Simulating the seasonal cycle of the Northern Hemisphere storm tracks using idealized nonlinear storm-track models. *J. Atmos. Sci.*, **64**, 2309–2331, <https://doi.org/10.1175/JAS3957.1>.
- , and W. Lin, 2011: Comments on “The role of the central Asian mountains on the midwinter suppression of North Pacific storminess.” *J. Atmos. Sci.*, **68**, 2800–2803, <https://doi.org/10.1175/JAS-D-11-021.1>.
- , and Y. Guo, 2012: Is Pacific storm-track activity correlated with the strength of upstream wave seeding? *J. Climate*, **25**, 5768–5776, <https://doi.org/10.1175/JCLI-D-11-00555.1>.
- , S. Lee, and K. L. Swanson, 2002: Storm track dynamics. *J. Climate*, **15**, 2163–2183, [https://doi.org/10.1175/1520-0442\(2002\)015<02163:STD>2.0.CO;2](https://doi.org/10.1175/1520-0442(2002)015<02163:STD>2.0.CO;2).
- Charney, J. G., 1947: The dynamics of long waves in a baroclinic westerly current. *J. Meteor.*, **4**, 136–162, [https://doi.org/10.1175/1520-0469\(1947\)004<0136:TDOLWI>2.0.CO;2](https://doi.org/10.1175/1520-0469(1947)004<0136:TDOLWI>2.0.CO;2).
- , and P. G. Drazin, 1961: Propagation of planetary-scale disturbances from the lower into the upper atmosphere. *J. Geophys. Res.*, **66**, 83–109, <https://doi.org/10.1029/JZ066i001p00083>.
- Chemke, R., 2017: Atmospheric energy transfer response to global warming. *Quart. J. Roy. Meteor. Soc.*, **143**, 2296–2308, <https://doi.org/10.1002/qj.3086>.
- Chen, G., I. M. Held, and W. A. Robinson, 2007: Sensitivity of the latitude of the surface westerlies to surface friction. *J. Atmos. Sci.*, **64**, 2899–2915, <https://doi.org/10.1175/JAS3995.1>.
- Christoph, M., U. Ulbrich, and P. Speth, 1997: Midwinter suppression of Northern Hemisphere storm track activity in the real atmosphere and in GCM experiments. *J. Atmos. Sci.*, **54**, 1589–1599, [https://doi.org/10.1175/1520-0469\(1997\)054<1589:MSONHS>2.0.CO;2](https://doi.org/10.1175/1520-0469(1997)054<1589:MSONHS>2.0.CO;2).
- Dee, D. P., and Coauthors, 2011: The ERA-Interim reanalysis: Configuration and performance of the data assimilation system. *Quart. J. Roy. Meteor. Soc.*, **137**, 553–597, <https://doi.org/10.1002/qj.828>.
- Deng, Y., and M. Mak, 2005: An idealized model study relevant to the dynamics of the midwinter minimum of the Pacific storm track. *J. Atmos. Sci.*, **62**, 1209–1225, <https://doi.org/10.1175/JAS3400.1>.
- Eady, E. T., 1949: Long waves and cyclone waves. *Tellus*, **1**, 33–52, <https://doi.org/10.3402/tellusa.v1i3.8507>.
- Edmon, H. J., B. J. Hoskins, and M. E. McIntyre, 1980: Eliassen–Palm cross sections for the troposphere. *J. Atmos. Sci.*, **37**,

- 2600–2616, [https://doi.org/10.1175/1520-0469\(1980\)037<2600:EPCSFT>2.0.CO;2](https://doi.org/10.1175/1520-0469(1980)037<2600:EPCSFT>2.0.CO;2).
- Fraedrich, K., E. Kirk, U. Luksch, and F. Lunkeit, 2005: The Portable University Model of the Atmosphere (PUMA): Storm track dynamics and low frequency variability. *Meteor. Z.*, **14**, 735–745, <https://doi.org/10.1127/0941-2948/2005/0074>.
- Frierson, D. M., 2007: The dynamics of idealized convection schemes and their effect on the zonally averaged tropical circulation. *J. Atmos. Sci.*, **64**, 1959–1976, <https://doi.org/10.1175/JAS3935.1>.
- Harnik, N., and E. K. Chang, 2004: The effects of variations in jet width on the growth of baroclinic waves: Implications for midwinter Pacific storm track variability. *J. Atmos. Sci.*, **61**, 23–40, [https://doi.org/10.1175/1520-0469\(2004\)061<0023:TEOVJ>2.0.CO;2](https://doi.org/10.1175/1520-0469(2004)061<0023:TEOVJ>2.0.CO;2).
- James, I. N., 1987: Suppression of baroclinic instability in horizontally sheared flows. *J. Atmos. Sci.*, **44**, 3710–3720, [https://doi.org/10.1175/1520-0469\(1987\)044<3710:SOBIIIH>2.0.CO;2](https://doi.org/10.1175/1520-0469(1987)044<3710:SOBIIIH>2.0.CO;2).
- , 1994: *Introduction to Circulating Atmospheres*. Cambridge University Press, 230 pp.
- Källberg, P., P. Berrisford, B. Hoskins, A. Simmons, S. Uppala, S. Lamy-Thépaut, and R. Hine, 2005: ERA-40 Atlas. ERA-40 Project Rep. Series 19, ECMWF, 199 pp.
- Kang, S. M., and J. Lu, 2012: Expansion of the Hadley cell under global warming: Winter versus summer. *J. Climate*, **25**, 8387–8393, <https://doi.org/10.1175/JCLI-D-12-00323.1>.
- Kaspi, Y., and T. Schneider, 2011: Downstream self-destruction of storm tracks. *J. Atmos. Sci.*, **68**, 2459–2464, <https://doi.org/10.1175/JAS-D-10-05002.1>.
- , and —, 2013: The role of stationary eddies in shaping midlatitude storm tracks. *J. Atmos. Sci.*, **70**, 2596–2613, <https://doi.org/10.1175/JAS-D-12-082.1>.
- Lachmy, O., and N. Harnik, 2014: The transition to a subtropical jet regime and its maintenance. *J. Atmos. Sci.*, **71**, 1389–1409, <https://doi.org/10.1175/JAS-D-13-0125.1>.
- , and —, 2016: Wave and jet maintenance in different flow regimes. *J. Atmos. Sci.*, **73**, 2465–2484, <https://doi.org/10.1175/JAS-D-15-0321.1>.
- Lee, S.-S., J.-Y. Lee, K.-J. Ha, B. Wang, A. Kitoh, Y. Kajikawa, and M. Abe, 2013: Role of the Tibetan Plateau on the annual variation of mean atmospheric circulation and storm-track activity. *J. Climate*, **26**, 5270–5286, <https://doi.org/10.1175/JCLI-D-12-00213.1>.
- Lehmann, J., D. Coumou, K. Frieler, A. V. Eliseev, and A. Levermann, 2014: Future changes in extratropical storm tracks and baroclinicity under climate change. *Environ. Res. Lett.*, **9**, 084002, <https://doi.org/10.1088/1748-9326/9/8/084002>.
- Levine, X. J., and T. Schneider, 2015: Baroclinic eddies and the extent of the Hadley circulation: An idealized GCM study. *J. Atmos. Sci.*, **72**, 2744–2761, <https://doi.org/10.1175/JAS-D-14-0152.1>.
- Lorenz, E. N., 1955: Available potential energy and the maintenance of the general circulation. *Tellus*, **7**, 157–167, <https://doi.org/10.3402/tellusa.v7i2.8796>.
- Mbengue, C., and T. Schneider, 2013: Storm track shifts under climate change: What can be learned from large-scale dry dynamics. *J. Climate*, **26**, 9923–9930, <https://doi.org/10.1175/JCLI-D-13-00404.1>.
- , and —, 2017: Storm-track shifts under climate change: Toward a mechanistic understanding using baroclinic mean available potential energy. *J. Atmos. Sci.*, **74**, 93–110, <https://doi.org/10.1175/JAS-D-15-0267.1>.
- Merlis, T. M., T. Schneider, S. Bordoni, and I. Eisenman, 2013: Hadley circulation response to orbital precession. Part I: Aquaplanets. *J. Climate*, **26**, 740–753, <https://doi.org/10.1175/JCLI-D-11-00716.1>.
- Nakamura, H., 1992: Midwinter suppression of baroclinic wave activity in the Pacific. *J. Atmos. Sci.*, **49**, 1629–1642, [https://doi.org/10.1175/1520-0469\(1992\)049<1629:MSOBWA>2.0.CO;2](https://doi.org/10.1175/1520-0469(1992)049<1629:MSOBWA>2.0.CO;2).
- , and T. Sampe, 2002: Trapping of synoptic-scale disturbances into the North-Pacific subtropical jet core in midwinter. *Geophys. Res. Lett.*, **29**, 1761, <https://doi.org/10.1029/2002GL015535>.
- , and A. Shimpo, 2004: Seasonal variations in the Southern Hemisphere storm tracks and jet streams as revealed in a reanalysis dataset. *J. Climate*, **17**, 1828–1844, [https://doi.org/10.1175/1520-0442\(2004\)017<1828:SVITSH>2.0.CO;2](https://doi.org/10.1175/1520-0442(2004)017<1828:SVITSH>2.0.CO;2).
- , T. Izumi, and T. Sampe, 2002: Interannual and decadal modulations recently observed in the Pacific storm track activity and East Asian winter monsoon. *J. Climate*, **15**, 1855–1874, [https://doi.org/10.1175/1520-0442\(2002\)015<1855:IADMRO>2.0.CO;2](https://doi.org/10.1175/1520-0442(2002)015<1855:IADMRO>2.0.CO;2).
- Novak, L., M. H. P. Ambaum, and R. Tailleux, 2017: Marginal stability and predator-prey behaviour within storm tracks. *Quart. J. Roy. Meteor. Soc.*, **143**, 1421–1433, <https://doi.org/10.1002/qj.3014>.
- O’Gorman, P. A., 2010: Understanding the varied response of the extratropical storm tracks to climate change. *Proc. Natl. Acad. Sci. USA*, **107**, 19 176–19 180, <https://doi.org/10.1073/pnas.1011547107>.
- , and T. Schneider, 2008a: Energy of midlatitude transient eddies in idealized simulations of changed climates. *J. Climate*, **21**, 5797–5806, <https://doi.org/10.1175/2008JCLI2099.1>.
- , and —, 2008b: The hydrological cycle over a wide range of climates simulated with an idealized GCM. *J. Climate*, **21**, 3815–3832, <https://doi.org/10.1175/2007JCLI2065.1>.
- Park, H.-S., J. C. Chiang, and S.-W. Son, 2010: The role of the central Asian mountains on the midwinter suppression of North Pacific storminess. *J. Atmos. Sci.*, **67**, 3706–3720, <https://doi.org/10.1175/2010JAS3349.1>.
- Penny, S., G. H. Roe, and D. S. Battisti, 2010: The source of the midwinter suppression in storminess over the North Pacific. *J. Climate*, **23**, 634–648, <https://doi.org/10.1175/2009JCLI2904.1>.
- Robinson, D. P., and R. X. Black, 2005: The statistics and structure of subseasonal midlatitude variability in NASA GSFC GCMs. *J. Climate*, **18**, 3294–3316, <https://doi.org/10.1175/JCLI3450.1>.
- Schemm, S., and T. Schneider, 2018: Eddy lifetime, number, and diffusivity and the suppression of eddy kinetic energy in midwinter. *J. Climate*, **31**, 5649–5665, <https://doi.org/10.1175/JCLI-D-17-0644.1>.
- Schneider, T., 2004: The tropopause and the thermal stratification in the extratropics of a dry atmosphere. *J. Atmos. Sci.*, **61**, 1317–1340, [https://doi.org/10.1175/1520-0469\(2004\)061<1317:TTATTS>2.0.CO;2](https://doi.org/10.1175/1520-0469(2004)061<1317:TTATTS>2.0.CO;2).
- , 2006: The general circulation of the atmosphere. *Annu. Rev. Earth Planet. Sci.*, **34**, 655–688, <https://doi.org/10.1146/annurev.earth.34.031405.125144>.
- , 2010: Water vapor and the dynamics of climate changes. *Rev. Geophys.*, **48**, RG3001, <https://doi.org/10.1029/2009RG000302>.
- , and C. C. Walker, 2006: Self-organization of atmospheric macroturbulence into critical states of weak nonlinear eddy–eddy interactions. *J. Atmos. Sci.*, **63**, 1569–1586, <https://doi.org/10.1175/JAS3699.1>.
- , and —, 2008: Scaling laws and regime transitions of macroturbulence in dry atmospheres. *J. Atmos. Sci.*, **65**, 2153–2173, <https://doi.org/10.1175/2007JAS2616.1>.

- Simmons, A. J., and B. J. Hoskins, 1978: The lifecycle of some baroclinic waves. *J. Atmos. Sci.*, **35**, 414–432, [https://doi.org/10.1175/1520-0469\(1978\)035<0414:TLCOSN>2.0.CO;2](https://doi.org/10.1175/1520-0469(1978)035<0414:TLCOSN>2.0.CO;2).
- Solomon, A. B., 1997: An observational study of the spatial and temporal scales of transient eddy sensible heat fluxes. *J. Climate*, **10**, 508–520, [https://doi.org/10.1175/1520-0442\(1997\)010<0508:AOSOTS>2.0.CO;2](https://doi.org/10.1175/1520-0442(1997)010<0508:AOSOTS>2.0.CO;2).
- Son, S.-W., M. Ting, and L. M. Polvani, 2009: The effect of topography on storm-track intensity in a relatively simple general circulation model. *J. Atmos. Sci.*, **66**, 393–411, <https://doi.org/10.1175/2008JAS2742.1>.
- Thorncroft, C. D., B. J. Hoskins, and M. E. McIntyre, 1993: Two paradigms of baroclinic wave life-cycle behaviour. *Quart. J. Roy. Meteor. Soc.*, **119**, 17–55, <https://doi.org/10.1002/qj.49711950903>.
- Vallis, G. K., P. Zurita-Gotor, C. Cairns, and J. Kidston, 2015: Response of the large-scale structure of the atmosphere to global warming. *Quart. J. Roy. Meteor. Soc.*, **141**, 1479–1501, <https://doi.org/10.1002/qj.2456>.
- Walker, C. C., and T. Schneider, 2006: Eddy influences on Hadley circulations: Simulations with an idealized GCM. *J. Atmos. Sci.*, **63**, 3333–3350, <https://doi.org/10.1175/JAS3821.1>.
- Yin, J. H., 2002: The peculiar behavior of baroclinic waves during the midwinter suppression of the Pacific storm track. Ph.D. thesis, University of Washington, 121 pp., <http://hdl.handle.net/1773/10043>.
- Yuval, J., H. Afargan, and Y. Kaspi, 2018: The relation between the seasonal changes in jet characteristics and the Pacific midwinter minimum in eddy activity. *Geophys. Res. Lett.*, **45**, 9995–10 002, <https://doi.org/10.1029/2018GL078678>.
- Zhang, Y., and I. M. Held, 1999: A linear stochastic model of a GCM's midlatitude storm tracks. *J. Atmos. Sci.*, **56**, 3416–3435, [https://doi.org/10.1175/1520-0469\(1999\)056<3416:ALSMOA>2.0.CO;2](https://doi.org/10.1175/1520-0469(1999)056<3416:ALSMOA>2.0.CO;2).